Giant Pressure Dependence and Dimensionality Switching in a Metal-Organic Quantum Antiferromagnet

B. Wehinger, C. Fiolka, A. Lanza, R. Scatena, M. Kubus, A. Grockowiak, W. A. Coniglio, D. Graf, M. Skoulatos, J.-H. Chen, J. Gukelberger, N. Casati, O. Zaharko, P. Macchi, K. W. Krämer, S. Tozer, C. Mudry, B. Normand, and Ch. Rüegg

Phys. Rev. Lett. **121**, 117201 — Published 11 September 2018

DOI: 10.1103/PhysRevLett.121.117201

Giant pressure dependence and dimensionality switching in a metal-organic quantum antiferromagnet

B. Wehinger,[1,2,*] C. Fiolka,[3] A. Lanza,[3] R. Scatena,[3] M. Kubus,[3] A. Grockowiak,[4] W. A. Coniglio,[4] D. Graf,[4] M. Skoulatos,[5] J.-H. Chen,[6,7] J. Gukelberger,[7,8] N. Casati,[9] O. Zaharko,[2] P. Macchi,[3] K. W. Krämer,[3] S. Tozer,[4] C. Mudry,[6] B. Normand,[10] and Ch. Rüegg[1,10]

[1] *Department of Quantum Matter Physics, University of Geneva, 24, Quai Ernest Ansermet, CH-1211 Genève, Switzerland*
[2] *Laboratory for Neutron Scattering and Imaging, Paul Scherrer Institute, CH-5232 Villigen-PSI, Switzerland*
[3] *Department of Chemistry and Biochemistry, University of Bern, Freiestrasse 3, CH-3012 Bern, Switzerland*
[4] *National High Magnetic Field Laboratory, 1800 E. Paul Dirac Drive, Tallahassee, FL 32310, USA*
[5] *Heinz-Maier-Leibnitz Zentrum and Physics Department, Technische Universität München, Lichtenbergstr. 1, 85748 Garching, Germany*
[6] *Condensed Matter Theory Group, Paul Scherrer Institute, CH-5232 Villigen-PSI, Switzerland*
[7] *Theoretical Physics, ETH Zürich, CH-8093 Zürich, Switzerland*
[8] *Département de Physique and Institut Quantique, Université de Sherbrooke, Sherbrooke, Québec, J1K 2R1, Canada*
[9] *Swiss Light Source, Paul Scherrer Institute, CH-5232 Villigen-PSI, Switzerland*
[10] *Neutrons and Muons Research Division, Paul Scherrer Institute, CH-5232 Villigen-PSI, Switzerland*

(Dated: June 11, 2018)

We report an extraordinary pressure dependence of the magnetic interactions in the metal-organic system [$(CuF_2(H_2O)_2)_2$pyrazine]. At zero pressure, this material realizes a quasi-two-dimensional (Q2D) spin-1/2 square-lattice Heisenberg antiferromagnet. By high-pressure, high-field susceptibility measurements we show that the dominant exchange parameter is reduced continuously by a factor of 2 on compression. Above 18 kbar, a phase transition occurs, inducing an orbital reordering that switches the dimensionality, transforming the Q2D lattice into weakly coupled chains (Q1D). We explain the microscopic mechanisms for both phenomena by combining detailed x-ray and neutron diffraction studies with quantitative modeling using spin-polarized density functional theory.

Quantum fluctuations are especially strong in low-dimensional systems, giving rise to numerous exotic phenomena in quantum magnetism [1–3]. The design and control of materials with quasi-one- (Q1D) and quasi-two-dimensional (Q2D) antiferromagnetic (AFM) interactions is of particular interest for potential applications in AFM spintronics, where energy efficiencies are outstanding compared to ferromagnets and the spin dynamics is faster by orders of magnitude [4–6]. A full exploitation of this potential requires further progress in theoretical, experimental, and materials physics, specifically designer low-dimensional materials with experimentally controlled magnetic exchange to benchmark accurate theoretical descriptions.

Metal-organic compounds based on Cu^{2+} ions make excellent model quantum magnets because of their localized spin-1/2 moments and large charge gap. Suitable materials are based on soft coordination polymers with rigid linkers such as pyrazine (pyz), which provide Cu^{2+} networks with exchange parameters on the scale of 0.1-10 K that are robust and strongly anisotropic in space [7, 8]. These interactions can be determined to high accuracy from thermodynamic and spectroscopic measurements, and interaction control can be achieved by chemistry or physics. Chemical variation of ligands and counter-ions allows for significant modification [9, 10], to the point of dimensionality control [11], while fine-tuning is possible by isotopic substitution [12]. Physically, an applied pressure provides direct control of structural and, in turn, magnetic properties [13, 14].

In this Letter, we report on two types of extreme behavior in [$(CuF_2(H_2O)_2)_2$pyz] under pressure. Magnetic susceptibility measurements show massive and continuous changes of the dominant exchange parameters in two different low-dimensional magnetic states. These states, a Q2D spin-1/2 square-lattice antiferromagnet at pressures up to 18 kbar and Q1D AFM chains at higher pressures, are separated by a phase transition which switches the magnetic orbital and thus the dimensionality. By diffraction studies and quantitative modeling using spin-polarized density functional theory (DFT), we show that its origin lies in the pressure-sensitivity of superexchange paths involving water ligands. Our results allow unprecedented control of magnetic interactions and thus represent an important step towards materials choices for quantum magnetism by design.

Single crystals of [$(CuF_2(H_2O)_2)_2$pyz] were grown as described in Sec. S1 of the Supplemental Material (SM) [15]. Magnetic susceptibility measurements were performed using a Tunnel Diode Oscillator (TDO), as detailed in Sec. S2 of the SM [15], while the magnetic exchange was controlled by isotropic compression of a sam-

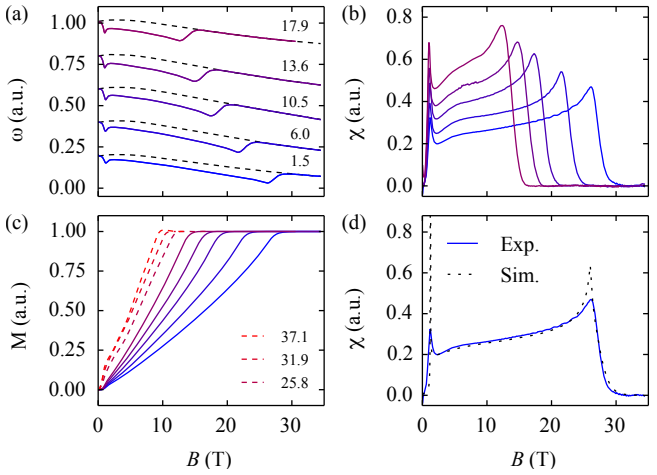

FIG. 1. (a) Measured TDO resonance frequencies, ω, at selected pressures, P, for $T = 1.5$ K (solid lines), shown with the magnetoresistive background of the resonator coil (dashed). (b) $\chi(B)$ for the same T and P values. (c) $M(B)$ at $P = 37.1$, 31.9, and 25.8 kbar (dashed lines), measured at 0.4 K, and at the pressures shown in panels (a) and (b) (full lines), measured at 1.5 K. (d) $\chi(B)$ at 1.5 kbar and 1.5 K as obtained from experiment (full line) and from QMC simulations (dashed line).

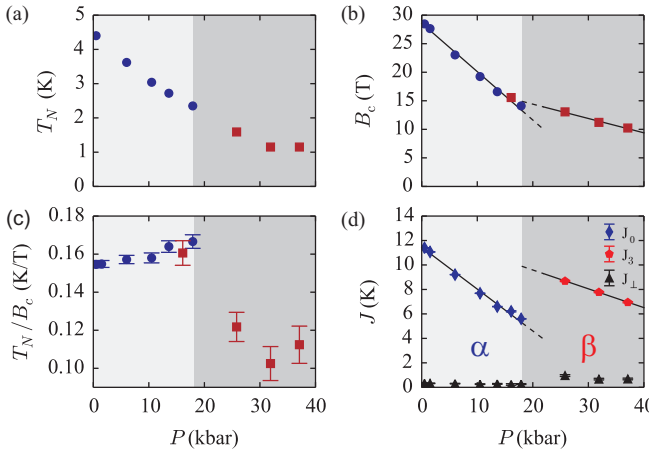

FIG. 2. (a) T_N measured as a function of P at field values corresponding to $B_{\rm sf}$. (b) B_c obtained from self-consistent fitting procedure; black lines show linear fits. Blue circles show data obtained using the piston cell, red squares using the Moissanite cell. (c) Ratio T_N/B_c as a function of P, illustrating the evolution of dimensionality; the sharp drop marks the phase transition to the Q1D magnetic system. Two missing values of T_N for calculating T_N/B_c were obtained from linear interpolation based on panel (a). (d) Exchange parameters obtained from QMC fits to the experimental data, shown together with a linear fit (black lines).

ple aligned with the crystallographic a axis parallel to the field. We performed two independent experiments using (i) a piston cylinder cell for pressures up to 17.9 kbar in fields up to 35 T and temperatures down to 1.5 K and (ii) a specially designed Moissanite anvil cell for pressures up to 37.1 kbar with maximum field 18 T and minimum temperature 0.4 K.

The TDO resonance frequency, ω, is shown in Fig. 1(a) as a function of field at five different pressures and a constant temperature of 1.5 K. The magnetic susceptibility, $\chi = \partial M/\partial B$ in Fig. 1(b), was obtained by subtracting the magnetoresistive background of the resonator coil from ω. The peak observed at low fields is due to a spin-flop transition, which occurs at $B_{\rm sf} = 1.2$ T at 1.5 kbar and shifts to 1.0 T at 17.9 kbar, then from 0.84 T at 25.8 kbar to 0.7 T at 37.1 kbar. Otherwise $\chi(B)$ shows a gradual increase with field and a pronounced peak prior to saturation. The magnetization, M [Fig. 1(c)], obtained by integrating $\chi(B)$, changes little for fields below $B_{\rm sf}$, then shows increasing field-alignment up to a saturation field, B_c, that changes dramatically with pressure.

The Néel temperature, T_N in Fig. 2(a), was determined by measuring the temperature dependence of ω at the field $B = B_{\rm sf}$ corresponding to each pressure point. This allows for a precise measurement because the changes are particularly pronounced at T_N (Sec. S2 of the SM [15]). The relative change of T_N with pressure is also dramatic, and its continuous change over such a wide pressure range is quite unprecedented. Because T_N is a significant fraction of our measurement temperature, care is required to extract the underlying magnetic exchange parameters and we adopt the consistent fitting procedure described next.

At low pressures, $[(CuF_2(H_2O)_2)_2pyz]$ is a prototypical spin-1/2 square-lattice antiferromagnet with dominant in-plane magnetic exchange, J_0, and weak interlayer interactions [14]. We observe that $[(CuF_2(H_2O)_2)_2pyz]$ has three interlayer exchange parameters and analyze J_1, J_2, and J_3 in connection with Fig. 3, but to complete the experimental analysis we combine them as follows. We have performed neutron diffraction measurements of the magnetic structure of $[(CuF_2(H_2O)_2)_2pyz]$, detailed in Sec. S3 of the SM [15], which establish that the interbilayer coupling, J_1, is AFM while the effective intrabilayer coupling, $\tilde{J}_2$, which is a combination of J_2 and J_3, is effectively FM. Within the mean-field Random Phase Approximation (RPA) treatment [28] summarized in Sec. S5 of the SM [15], one may show that only the sum $|J_1|+|\tilde{J}_2| = 2J_\perp$ enters the susceptibility, and hence extract a single effective interlayer exchange parameter, $J_\perp$.

For a full investigation of pressure dependence, we note that $g\mu_B B_c(P) = 4J_0(P) + 2J_\perp(P)$ is the sum of all interaction strengths at a single Cu^{2+} site, with $g = 2.42$ determined experimentally for $\boldsymbol{B} \parallel \boldsymbol{a}$ [14]. $J_0(P)$ and $T_N(P)$ can be used to determine one interlayer exchange parameter by employing the empirical relation

$$J_\perp(P) = J_0(P)\, e^{b-4\pi\rho_s/T_N(P)}, \qquad (1)$$

developed from quantum Monte Carlo (QMC) simulations for the spin-1/2 Q2D AFM Heisenberg model [27], where $b = 2.43$ is a non-universal constant and $\rho_s = 0.183 J_0$ is the spin stiffness. This equation is valid for $0.001 \leq J_\perp/J_0 \leq 1$ and is obtained from a modified RPA (Sec. S5 of the SM [15]).

From the zero-temperature estimates provided by these equations, we obtain self-consistent values for $J_0(P)$ and $J_\perp(P)$ by computing $\chi(B)$ at the temperatures of our measurements. We perform QMC simulations using the ALPS open-source code [38], as detailed in Sec. S6 of the SM [15]. The results of Fig. 1(b) can be reproduced with quantitative accuracy at all fields and pressures by using a nearest-neighbor XXZ Hamiltonian on a simple cubic lattice, as illustrated in Fig. 1(d) for the data at $P = 1.5$ kbar. The spin-flop transition means that the SU(2) spin symmetry is broken down to U(1), and the measured $B_{\rm sf}$ value is obtained by setting $\Delta J_0^z = J_0^z - J_0 = 0.09$ K, i.e. with a 1% easy-axis anisotropy in J_0.

We show our results for $B_c(P)$ in Fig. 2(b) and for $J_0(P)$ and $J_\perp(P)$ in Fig. 2(d). Linear fits for the low-pressure α phase yield $J_0(P) = 11.4(1)\,\mathrm{K} - 0.34(1)\,P\,\mathrm{K/kbar}$ and $J_\perp(P) = 0.33(1)\,\mathrm{K} - 0.005(1)\,P\,\mathrm{K/kbar}$. As we quantify below, such a large coefficient for J_0 is quite extraordinary. In Fig. 2(c) we show the ratio T_N/B_c as a function of pressure. Mean-field arguments predict both T_N and B_c to be proportional to the sum of all interactions and hence their ratio to be constant. However, quantum fluctuations in low-dimensional systems suppress T_N (to zero in the 1D and 2D limits) but not B_c. Our results imply that the Q2D system becomes slightly more 3D (i.e. $J_\perp/J_0$ increases) with increasing pressure up to 18 kbar.

The discontinuous change at 18 kbar marks a transition to a different low-dimensional magnetic phase. We find (below) that it is caused by a structural phase transition to a high-pressure β phase. Here, the J_3 exchange becomes dominant, defining a system of AFM spin-1/2 chains, while $J_\perp$ corresponds to the arithmetic mean of J_0, J_1, and J_2. For this Q1D case one has $g\mu_B B_c = 2J_3 + 4J_\perp$ and

$$J_\perp = T_N/[4c\sqrt{\ln(lJ_3/T_N) + 0.5\ln(\ln(lJ_3/T_N))}], \quad (2)$$

where $c = 0.233$ and $l = 2.6$ [27]. Once again we constrain in interchain couplings by RPA arguments [15] and refine self-consistent values for $J_3(P)$ and $J_\perp(P)$ in the β phase by QMC simulations. Linear fits to the results shown in Fig. 2(d) yield $J_3(P) = 12.7(1)\,\mathrm{K} - 0.15(1)\,P\,\mathrm{K/kbar}$ and $J_\perp(P) = 1.6(5)\,\mathrm{K} - 0.03(1)\,P\,\mathrm{K/kbar}$; the coefficient of $J_3(P)$ is again anomalously large.

To place these results in context and to justify our use of "extraordinary," we stress that compressive effects on magnetic exchange are expected due to reduced orbital separations and altered bond angles. These effects are generally at the 1% level in inorganic materials and the 10% level in organic ones. By "giant pressure dependence" we refer to far larger effects. Because a structural phase transition may, rather obviously, cause dramatic changes, we focus on continuous processes. Unusually large (10%) pressure effects known in inorganic systems [39, 40] rely on proximity to a 90-degree bonding geometry. On a scale where our "pressure factor" is 2, the most extreme values we have found in organic materials range from 1.4 to 1.67 [41–44]; we are not aware of any microscopic explanations for these results. Here we demonstrate that our observations are explained by an unconventional mechanism where the spin density evolves continuously between two different atomic orbitals, rather than remaining in one orbital whose shape changes slightly.

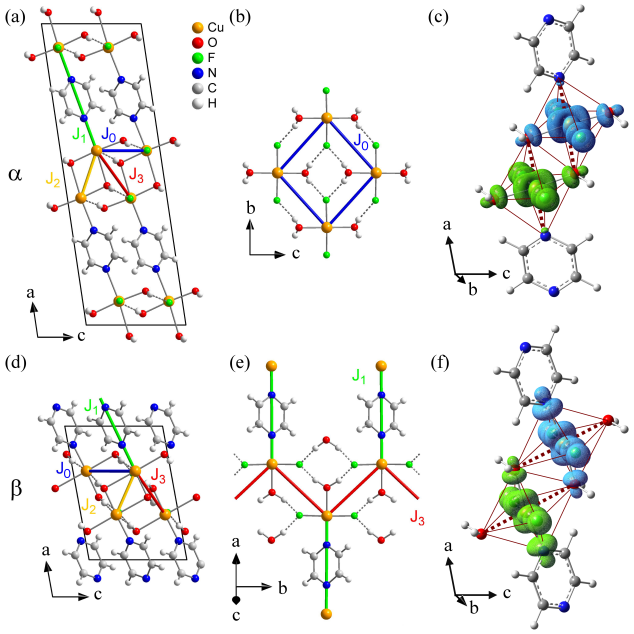

FIG. 3. Crystallographic structure of $[(CuF_2(H_2O)_2)_2pyz]$ in the α phase, showing (a) the ac and (b) the bc plane. The dominant exchange parameter, J_0, is mediated by Cu-O-H$\cdots$F-Cu superexchange paths. (c) Calculated spin-density distribution of the ground state, with spins up and down represented respectively in cyan and green. Red lines mark the coordination octahedron of the Cu^{2+} ions and thick dashed lines the pseudo-Jahn-Teller axis. Structure in the β phase, showing (d) the ac and (e) the ab plane. The dominant exchange parameter, J_3, is mediated by Cu-O-H$\cdots$F-Cu paths. (f) Spin density distribution; both the pseudo-Jahn-Teller axis and the magnetic orbitals are reoriented at the phase transition.

To understand our results we have performed structural investigations by x-ray diffraction in order to benchmark first-principles calculations using spin-polarized DFT. As detailed in Sec. S4 of the SM [15], we made high-pressure single-crystal x-ray diffraction measurements at ambient temperature and powder measurements at 5 K.

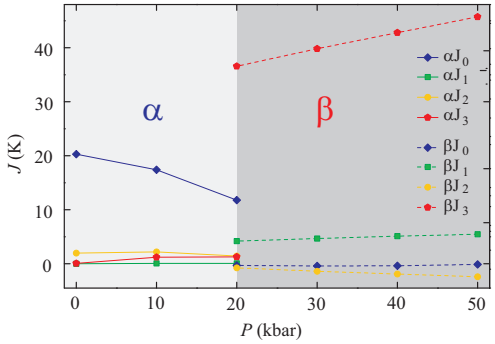

FIG. 4. Exchange parameters calculated as function of pressure for the α and β phases using spin-polarized DFT.

The unit-cell parameters and bond distances for different pressures are reported in Tables S1 and S2 of the SM [15] and full structural details are provided as crystallographic information files (CIFs). As represented in Fig. 3, Cu^{2+} ions are linked by OH$\cdots$F hydrogen bonds to form distorted square-lattice layers in the *bc* plane. H_2O ligands further connect these into a bilayer and pyz molecules link the bilayers into a 3D coordination network. In the α phase [Figs. 3(a)-3(c)], the asymmetry in Cu coordination between the intralayer Cu^{2+}-Cu^{2+} bonds and the interlayer H_2O-Cu-pyrazine direction is referred to as "pseudo-Jahn-Teller". Upon compression, both axial ligand bonds are shortened progressively. Because of the stronger field of the pyz ligand, the decreasing length of the Cu-N bond (from 2.40 to 2.30 Å, Table S2) is expected to have a stronger effect on the metal stereochemistry, and indeed we will find that this decrease is responsible for the giant pressure dependence of J_0.

A structural phase transition was observed at 18 kbar. The high-pressure β phase, shown in Figs. 3(d)-3(f), is characterized by a dramatic reduction of the Cu-N bond to 2.1 Å and an even stronger rise in the intralayer Cu-O separation (Table S2). This structural rearrangement represents a switch of the pseudo-Jahn-Teller axis [Fig. 3(f)]. However, we note that the Cu-N distance remains longer than for regular pyrazine coordination (2.05 Å).

We use the lattice symmetry and approximate atomic positions at ambient pressure as input for geometry optimizations within periodic DFT calculations, which we perform using CRYSTAL14 [29] as outlined in Sec. S7 of the SM [15]. These reproduce all of the observed structural features, including their evolution with pressure. They demonstrate that the β phase is more stable than α for pressures above 18 kbar, i.e. the DFT calculations provide quantitative agreement on the critical pressure for the structural transition.

To investigate magnetic exchange in $[(CuF_2(H_2O)_2)_2pyz]$, we identify the four Cu-Cu pathways shown in Fig. 3. We obtain the exchange parameters from the energy differences between high- and low-spin states of dinuclear fragments, calculated using the GAUSSIAN09 package [33] with the procedure described in Ref. [35] and summarized in Sec. S7 of the SM [15]. We find that the Cu^{2+} ions have the highest spin densities, with the remaining fraction delocalized on the ligands. In the α phase, the magnetic orbitals involve F^- and H_2O ligands [Fig. 3(c)] and the primary contribution to J_0 is from superexchange via Cu-O-H$\cdots$F-Cu paths, making Q2D magnetic layers that match the structural square lattice (Fig. 3(b) and Ref. [25]). The other exchange paths, marked J_1, J_2, and J_3 in Fig. 3(a), are poorly directed relative to the magnetic orbital and are small.

The calculated magnetic exchange parameters are shown in Fig. 4. DFT calculations without explicit account of correlation effects cannot in general obtain exchange parameters with quantitative accuracy, but their qualitative features contain essential physical insight. Most importantly, the giant decrease of J_0 in the α phase is in good qualitative agreement with experiment [Fig. 2(d)]. Its microscopic origin lies primarily in the decrease of the axial Cu-N distance, which causes a systematic reduction of the equatorial spin density of the magnetic orbital [Fig. 3(c)]. DFT indicates further that all of the subdominant exchange parameters are small. Although this places them below the resolution limits of our calculations [45], it also supports the experimental analysis above. We draw attention to the trend visible in DFT that compression of the axial bonds enhances J_3 strongly, from 60 mK at ambient pressure to 1.3 K at 20 kbar, without affecting J_1 or J_2 significantly.

In the β phase, the magnetic orbital revealed by the DFT spin density encompasses the two F^- ions and the (formerly axial) interlayer water and pyz ligands [Fig. 3(f)]. This orbital reorientation corresponds to the switch of the pseudo-Jahn-Teller axis and is responsible for the massive jumps in all of the exchange parameters (Fig. 4). J_3 becomes dominant [Fig. 3(e)], while J_1 is significantly smaller (by a factor of 9 in our calculations). J_0 and J_2 are weaker still, because they involve water ligands lying normal to the magnetic orbital [Fig. 3(f)], and hence the system becomes Q1D. This pressure-induced switching of orbital orientation and system dimensionality is analogous to the transitions reported for the "monolayer" material $[CuF_2(H_2O)_2pyz]$ [46, 47] and occurs despite the less symmetric Cu^{2+} coordination of $[(CuF_2(H_2O)_2)_2pyz]$. The monolayer system shows a relatively weak continuous pressure effect (17%) [48] and no microscopic analysis of the magnetic interactions was provided.

Thus our combined experimental and theoretical results both demonstrate unequivocally and explain qualitatively the dramatic changes in the magnetic properties of $[(CuF_2(H_2O)_2)_2pyz]$ under applied hydrostatic pressure. There are two quite different phenomena, namely

(i) the giant but continuous decrease of the magnetic coupling within the square lattice in the α phase and (ii) a discontinuous switching of the dimensionality of magnetic exchange at 18 kbar. Our calculations show that the key structural feature explaining (i) is the compression of bonds along the pseudo-Jahn-Teller axis, which causes a progressive redistribution of spin density in the magnetic orbital driving a strong and systematic reduction of the in-plane exchange. (ii) is driven by an abrupt switch in orientation of this orbital, favoring the intrabilayer exchange path J_3, which establishes a Q1D magnetic network and explains the especially low T_N/B_c in Fig. 2(c).

While our first-principles structural calculations for $[(CuF_2(H_2O)_2)_2pyz]$ under pressure are reliable at a quantitative level, our spin-dependent energetic calculations are not. Nevertheless, they do reproduce correctly the order of importance and the ratios of the exchange parameters at all pressures on both sides of the transition [Figs. 4 and 2(d)]. One key qualitative point is the DFT insight into the hierarchy of exchange parameters, and specifically the fact that only one is dominant, which allows us to disentangle the subdominant ones by experiment from a formalism based only on parameters J_0 or J_3 and $J_\perp$. However, DFT does predict an increase of J_3 with pressure in the β phase, in contrast to the decrease observed in experiment. We attribute this discrepancy to the limitations in our treatment of exchange correlations at the higher pressures. Finally, a particularly valuable feature of our DFT results is to show the relative contributions of the different ligands involved in the exchange processes, which is of vital importance in designing quantum magnets using metal-organic coordination polymers.

At a fundamental level, our experiments provide extreme sensitivity for investigating questions such as the evolution of entanglement in the many-body wavefunction, in particular close to quantum phase transitions. Neutron spectroscopy allows a direct probe of magnetic correlations and excitations. Recent measurements on $[CuF_2(H_2O)_2pyz]$ [49] revealed that the orbital reorientation induces a first-order transition of the magnetic excitations from spin waves to spinons. Our findings show that $[(CuF_2(H_2O)_2)_2pyz]$ is an even better candidate for such studies, not only because the key physics occurs at accessible pressure, field, and temperature conditions, but also because of the enormous range of parameter ratios spanned continuously by this material.

At a more applied level, our measurements make $[(CuF_2(H_2O)_2)_2pyz]$ an important model system for benchmarking any theoretical approach aiming to provide a quantitative description of magnetic properties from first principles. Our results afford direct insight into the toolkit of metal-organic chemistry, in terms of the ligands and linking units giving maximal flexibility and control of magnetic exchange. Thus they provide an important step towards designing quantum magnets for applications in AFM spintronics, where we anticipate that pressure effects will be created using multiferroic substrate materials. For such devices to be realized in layered heterostructures, it is critical that the dimensionality switching should leave the effective low-dimensional magnetic system in the plane of the layer, which is the case in $[(CuF_2(H_2O)_2)_2pyz]$ but not in $[CuF_2(H_2O)_2pyz]$.

In summary, we have observed and explained a giant pressure dependence of the magnetic exchange in the metal-organic quantum magnet $[(CuF_2(H_2O)_2)_2pyz]$. The combination of modern synthetic chemistry, high-precision physical measurements under extreme conditions, and state-of-the-art first-principles calculations allows essential calibration of theoretical methods and provides a promising strategy for designing quantum materials with tailored properties.

Acknowledgments. We thank R. Schwartz for professional engineering of the pressure cells and fixtures used for this study and acknowledge fruitful discussions with T. Giamarchi and N. Qureshi. Computations were performed at the Universities of Geneva and Bern on the Baobab and UBELIX clusters and using the resources of the Theory of Quantum Matter Group in Geneva. This research was supported by the EU FP7/2007-2013 under Grant No. 290605, the European Research Council (ERC) under the EU Horizon 2020 research and innovation programme Grant No. 681654, and the Swiss National Science Foundation (SNSF) under Grants No. 200020_150257 and 200020_162861, as well as through the SINERGIA Network "Mott Physics Beyond the Heisenberg Model". J.G. was supported by an SNSF Early Postdoc Mobility fellowship during part of this work and M.S. by TRR80 of the German Physical Society (DPG). We further acknowledge funding for measurements performed at the NHMFL by Grant No. DOE NNSA DE-NA0001979 with support by NSF Cooperative Agreement No. DMR-1157490 and the State of Florida.

* bjorn.wehinger@unige.ch

[1] E. Dagotto and T. M. Rice, Surprises on the way from one- to two-dimensional quantum magnets: The ladder materials, Science **271**, 618 (1996).

[2] B. Thielemann, C. Rüegg, H. M. Rønnow, A. M. Läuchli, J.-S. Caux, B. Normand, D. Biner, K. W. Krämer, H.-U. Güdel, J. Stahn, K. Habicht, K. Kiefer, M. Boehm, D. F. McMorrow, and J. Mesot, Direct observation of magnon fractionalization in the quantum spin ladder, Phys. Rev. Lett. **102**, 107204 (2009).

[3] L. Savary and L. Balents, Quantum spin liquids: a review, Rep. Prog. Phys. **80**, 016502 (2017).

[4] T. Jungwirth, X. Marti, P. Wadley, and J. Wunderlich, Antiferromagnetic spintronics, Nat. Nanotechnol. **11**, 231 (2016).

[5] T. Kosub, M. Kopte, R. Hühne, P. Appel, B. Shields, P. Maletinsky, R. Hübner, M. O. Liedke, J. Fassben-

der, O. G. Schmidt, and D. Makarov, Purely antiferromagnetic magnetoelectric random access memory, Nat. Commun. **8**, 13985 EP (2017).
[6] P. Wadley, B. Howells, J. Železný, C. Andrews, V. Hills, R. P. Campion, V. Novák, K. Olejník, F. Maccherozzi, S. S. Dhesi, S. Y. Martin, T. Wagner, J. Wunderlich, F. Freimuth, Y. Mokrousov, J. Kuneš, J. S. Chauhan, M. J. Grzybowski, A. W. Rushforth, K. W. Edmonds, B. L. Gallagher, and T. Jungwirth, Electrical switching of an antiferromagnet, Science **351**, 587 (2016).
[7] M. Conner, A. McConnell, J. Schlueter, and J. Manson, Structural and magnetic properties of copper(II) coordination polymers containing fluoride-based anions and ancillary organic ligands, J. Low Temp. Phys. **142**, 273 (2006).
[8] P. A. Goddard, J. Singleton, P. Sengupta, R. D. McDonald, T. Lancaster, S. J. Blundell, F. L. Pratt, S. Cox, N. Harrison, J. L. Manson, H. I. Southerland, and J. A. Schlueter, Experimentally determining the exchange parameters of quasi-two-dimensional Heisenberg magnets, New J. Phys. **10**, 083025 (2008).
[9] F. M. Woodward, P. J. Gibson, G. B. Jameson, C. P. Landee, M. M. Turnbull, and R. D. Willett, Two-dimensional Heisenberg antiferromagnets: syntheses, x-ray structures, and magnetic behavior of $[Cu(pz)_2](ClO_4)_2$, $[Cu(pz)_2](BF_4)_2$, and $[Cu(pz)_2(NO_3)](PF_6)$, Inorg. Chem. **46**, 4256 (2007).
[10] T. Lancaster, P. A. Goddard, S. J. Blundell, F. R. Foronda, S. Ghannadzadeh, J. S. Möller, P. J. Baker, F. L. Pratt, C. Baines, L. Huang, J. Wosnitza, R. D. McDonald, K. A. Modic, J. Singleton, C. V. Topping, T. A. W. Beale, F. Xiao, J. A. Schlueter, A. M. Barton, R. D. Cabrera, K. E. Carreiro, H. E. Tran, and J. L. Manson, Controlling magnetic order and quantum disorder in molecule-based magnets, Phys. Rev. Lett. **112**, 207201 (2014).
[11] P. A. Goddard, J. L. Manson, J. Singleton, I. Franke, T. Lancaster, A. J. Steele, S. J. Blundell, C. Baines, F. L. Pratt, R. D. McDonald, O. E. Ayala-Valenzuela, J. F. Corbey, H. I. Southerland, P. Sengupta, and J. A. Schlueter, Dimensionality selection in a molecule-based magnet, Phys. Rev. Lett. **108**, 077208 (2012).
[12] P. A. Goddard, J. Singleton, C. Maitland, S. J. Blundell, T. Lancaster, P. J. Baker, R. D. McDonald, S. Cox, P. Sengupta, J. L. Manson, K. A. Funk, and J. A. Schlueter, Isotope effect in quasi-two-dimensional metal-organic antiferromagnets, Phys. Rev. B **78**, 052408 (2008).
[13] J. L. Musfeldt, Z. Liu, S. Li, J. Kang, C. Lee, P. Jena, J. L. Manson, J. A. Schlueter, G. L. Carr, and M.-H. Whangbo, Pressure-induced local structure distortions in $Cu(pyz)F_2(H_2O)_2$, Inorg. Chem. **50**, 6347 (2011).
[14] A. Lanza, C. Fiolka, M. Fisch, N. Casati, M. Skoulatos, C. Rüegg, K. W. Krämer, and P. Macchi, New magnetic frameworks of $[(CuF_2(H_2O)_2)x(pyz)]$, Chem. Commun. **50**, 14504 (2014).
[15] For details see the supplemental material and Refs. [14, 16–37].
[16] C. T. Van Degrift, Tunnel diode oscillator for 0.001 ppm measurements at low temperatures, Rev. Sci. Instrum. **46**, 599 (1975).
[17] W. A. Coniglio, L. E. Winter, C. Rea, K. Cho, and C. Agosta, Improvements to the tunnel diode oscillator technique for high frequencies and pulsed magnetic fields with digital acquisition, arXiv:1003.5233 (2010).
[18] S. Ghannadzadeh, M. Coak, I. Franke, P. A. Goddard, J. Singleton, and J. L. Manson, Measurement of magnetic susceptibility in pulsed magnetic fields using a proximity detector oscillator, Rev. Sci. Instrum. **82**, 113902 (2011).
[19] D. E. Graf, R. L. Stillwell, K. M. Purcell, and S. W. Tozer, Nonmetallic gasket and miniature plastic turnbuckle diamond anvil cell for pulsed magnetic field studies at cryogenic temperatures, High Pressure Res. **31**, 533 (2011).
[20] K. Murata, K. Yokogawa, H. Yoshino, S. Klotz, P. Munsch, A. Irizawa, M. Nishiyama, K. Iizuka, T. Nanba, T. Okada, Y. Shiraga, and S. Aoyama, Pressure transmitting medium Daphne 7474 solidifying at 3.7 GPa at room temperature, Rev. Sci. Instrum. **79**, 085101 (2008).
[21] J. Rodrguez-Carvajal, Recent advances in magnetic structure determination by neutron powder diffraction, Physica B: Condensed Matter **192**, 55 (1993).
[22] CrysAlisPro 171.38.46 (2017).
[23] G. M. Sheldrick, Crystal structure refinement with SHELXL, Acta. Cryst. **C71**, 3 (2015).
[24] P. R. Willmott, D. Meister, S. J. Leake, M. Lange, A. Bergamaschi, M. Bo, U. Flechsig, F. Gozzo, B. Henrich, S. Ja, and R. Lu, The Materials Science beamline upgrade at the Swiss Light Source, J. Synchrotron Rad. **20**, 667 (2013).
[25] J. L. Manson, M. M. Conner, J. A. Schlueter, A. C. McConnell, H. I. Southerland, I. Malfant, T. Lancaster, S. J. Blundell, M. L. Brooks, F. L. Pratt, J. Singleton, R. D. McDonald, C. Lee, and M.-H. Whangbo, Experimental and theoretical characterization of the magnetic properties of $CuF_2(H_2O)_2(pyz)$ (pyz = pyrazine): A two-dimensional quantum magnet arising from supersuperexchange interactions through hydrogen bonded paths, Chem. Mater. **20**, 7408 (2008).
[26] S. Chakravarty, B. I. Halperin, and D. R. Nelson, Two-dimensional quantum Heisenberg antiferromagnet at low temperatures, Phys. Rev. B **39**, 2344 (1989).
[27] C. Yasuda, S. Todo, K. Hukushima, F. Alet, M. Keller, M. Troyer, and H. Takayama, Néel temperature of quasi-low-dimensional Heisenberg antiferromagnets, Phys. Rev. Lett. **94**, 217201 (2005).
[28] D. J. Scalapino, Y. Imry, and P. Pincus, Generalized Ginzburg-Landau theory of pseudo-one-dimensional systems, Phys. Rev. B **11**, 2042 (1975).
[29] R. Dovesi, V. R. Saunders, C. Roetti, R. Orlando, C. M. Zicovich-Wilson, F. Pascale, B. Civalleri, K. Doll, N. M. Harrison, I. J. Bush, P. D'Arco, M. Llunell, M. Causà, and Y. Noël, CRYSTAL14 User's Manual (2014).
[30] A. D. Becke, Density-functional thermochemistry. III. The role of exact exchange, J. Chem. Phys. **98**, 5648 (1993).
[31] C. Lee, W. Yang, and R. G. Parr, Development of the Colle-Salvetti correlation-energy formula into a functional of the electron density, Phys. Rev. B **37**, 785 (1988).
[32] C. Gatti, V. R. Saunders, and C. Roetti, Crystal field effects on the topological properties of the electron density in molecular crystals: The case of urea, J. Chem. Phys. **101**, 10686 (1994).
[33] M. J. Frisch, G. W. Trucks, H. B. Schlegel, G. E. Scuseria, M. A. Robb, J. R. Cheeseman, G. Scalmani,

V. Barone, B. Mennucci, H. N. G. A. Petersson, M. Caricato, X. Li, H. P. Hratchian, A. F. Izmaylov, J. Bloino, G. Zheng, J. L. Sonnenberg, M. Hada, M. Ehara, K. Toyota, R. Fukuda, J. Hasegawa, M. Ishida, T. Nakajima, Y. Honda, O. Kitao, H. Nakai, Vreven, T. Montgomery, J. A. Jr., J. E. Peralta, F. Ogliaro, M. Bearpark, J. J. Heyd, E. Brothers, K. N. Kudin, V. N. Staroverov, R. Kobayashi, J. Normand, K. Raghavachari, A. Rendell, J. C. Burant, S. S. Iyengar, J. Tomasi, M. Cossi, N. Rega, J. M. Millam, M. Klene, J. E. Knox, J. B. Cross, V. Bakken, C. Adamo, J. Jaramillo, R. Gomperts, R. E. Stratmann, O. Yazyev, A. J. Austin, R. Cammi, C. Pomelli, J. W. Ochterski, R. L. Martin, K. Morokuma, V. G. Zakrzewski, G. A. Voth, P. Salvador, J. J. Dannenberg, S. Dapprich, A. D. Daniels, Ö. Farkas, J. B. Foresman, J. V. Ortiz, J. Cioslowski, and D. J. Fox, Gaussian 09 (Gaussian, Inc.: Wallingford, CT, 2009).

[34] E. Ruiz, J. Cano, S. Alvarez, and P. Alemany, Broken symmetry approach to calculation of exchange coupling constants for homobinuclear and heterobinuclear transition metal complexes, J. Comput. Chem. **20**, 1391 (1999).

[35] L. H. R. D. Santos, A. Lanza, A. M. Barton, J. Brambleby, W. J. A. Blackmore, P. A. Goddard, F. Xiao, R. C. Williams, T. Lancaster, F. L. Pratt, S. J. Blundell, J. Singleton, J. L. Manson, and P. Macchi, Experimental and Theoretical Electron Density Analysis of Copper Pyrazine Nitrate Quasi-Low-Dimensional Quantum Magnets, J. Am. Chem. Soc. **138**, 2280 (2016).

[36] J. Brambleby, J. L. Manson, P. A. Goddard, M. B. Stone, R. D. Johnson, P. Manuel, J. A. Villa, C. M. Brown, H. Lu, S. Chikara, V. Zapf, S. H. Lapidus, R. Scatena, P. Macchi, Y.-s. Chen, L.-C. Wu, and J. Singleton, Combining microscopic and macroscopic probes to untangle the single-ion anisotropy and exchange energies in an $S = 1$ quantum antiferromagnet, Phys. Rev. B **95**, 134435 (2017).

[37] Y. Zhao and D. G. Truhlar, The M06 suite of density functionals for main group thermochemistry, thermochemical kinetics, noncovalent interactions, excited states, and transition elements: two new functionals and systematic testing of four M06-class functionals and 12 other functionals, Theor. Chem. Acc. **120**, 215 (2008).

[38] B. Bauer, L. D. Carr, H. G. Evertz, A. Feiguin, J. Freire, S. Fuchs, L. Gamper, J. Gukelberger, E. Gull, S. Guertler, A. Hehn, R. Igarashi, S. V. Isakov, D. Koop, P. N. Ma, P. Mates, H. Matsuo, O. Parcollet, G. Pawłowski, J. D. Picon, L. Pollet, E. Santos, V. W. Scarola, U. Schollwöck, C. Silva, B. Surer, S. Todo, S. Trebst, M. Troyer, M. L. Wall, P. Werner, and S. Wessel, The ALPS project release 2.0: open source software for strongly correlated systems, J. Stat. Mech.: Theory Exp. **2011**, P05001 (2011).

[39] M. Nishi, O. Fujita, J. Akimitsu, K. Kakurai, and Y. Fujii, High-pressure effects on the spin-Peierls compound $CuGeO_3$, Phys. Rev. B **52**, R6959 (1995).

[40] P. Merchant, B. Normand, K. W. Krämer, M. Boehm, D. F. McMorrow, and C. Rüegg, Quantum and classical criticality in a dimerized quantum antiferromagnet, Nat. Phys. **10**, 373 (2014).

[41] M. Mito, O. Fujita, M. Hitaka, T. Kawae, K. Takeda, S. Takagi, and H. Deguchi, Pressure Effects of an S = 1 Heisenberg Antiferromagnetic Bond Alternating Chain, J. Phys. Soc. Jpn. **70**, 1375 (2001).

[42] M. Mito, H. Akama, H. Deguchi, S. Takagi, T. Kawae, K. Takeda, T. Ishii, M. Yamashita, H. Nakao, Y. Murakami, and S. Yamamoto, Pressure Effects on an $S = 1$ Haldane Compound $Ni(C_5H_{14}N_2)_2N_3(PF_6)$, J. Phys. Soc. Jpn. **72**, 399 (2003).

[43] A. Sieber, D. Foguet-Albiol, O. Waldmann, S. T. Ochsenbein, G. Carver, H. Mutka, F. Fernandez-Alonso, M. Mezouar, H. P. Weber, G. Christou, and H. U. Güdel, Pressure dependence of the exchange interaction in the dimeric single-molecule magnet $[Mn_4O_3Cl_4(O_2CEt)_3(py)_3]_2$ from inelastic neutron scattering, Phys. Rev. B **74**, 024405 (2006).

[44] G. Seber, G. J. Halder, J. A. Schlueter, and P. M. Lahti, Pressure Effects on the Quasi-1-D Molecular Ferromagnet 2-(4,5,6,7-Tetrafluorobenzimidazol-2-yl)-4,4,5,5-tetramethyl-4,5-dihydro-1H-imidazole-3-oxide-1-oxyl, Crystal Growth & Design **11**, 4261 (2011).

[45] I. O. Thomas, S. J. Clark, and T. Lancaster, Exchange constants in molecule-based magnets derived from density functional methods, Phys. Rev. B **96**, 094403 (2017).

[46] G. J. Halder, K. W. Chapman, J. A. Schlueter, and J. L. Manson, Pressure-induced sequential orbital reorientation in a magnetic framework material, Angew. Chem., Int. Ed. **50**, 419 (2011).

[47] A. Prescimone, C. Morien, D. Allan, J. A. Schlueter, S. W. Tozer, J. L. Manson, S. Parsons, E. K. Brechin, and S. Hill, Pressure-driven orbital reorientations and coordination-sphere reconstructions in $[CuF_2(H_2O)_2(pyz)]$, Angew. Chem., Int. Ed. **51**, 7490 (2012).

[48] S. Ghannadzadeh, J. S. Möller, P. A. Goddard, T. Lancaster, F. Xiao, S. J. Blundell, A. Maisuradze, R. Khasanov, J. L. Manson, S. W. Tozer, D. Graf, and J. A. Schlueter, Evolution of magnetic interactions in a pressure-induced Jahn-Teller driven magnetic dimensionality switch, Phys. Rev. B **87**, 241102 (2013).

[49] M. Skoulatos, M. Månsson, C. Fiolka, K. W. Krämer, J. Schefer, J. S. White, and C. Rüegg, Dimensional reduction by pressure in the magnetic framework material $CuF_2(D_2O)_2(pyz)$: From spin-wave to spinon excitations, Phys. Rev. B **96**, 020414 (2017).